

Geometry of Deformed Cellular Spaces

SHLOMO BARAK¹ AND GEORGE SALMAN²

¹Taga Innovations, 18 Yosef Karo St., Tel Aviv 6701422, Israel

²School of Computer Science and Engineering, The Hebrew University of Jerusalem, Edmond J. Safra Campus, Jerusalem 9190401, Israel

* Corresponding author: George.salman@mail.huji.ac.il

Compiled March 5, 2026

We present an *Adaptive Geometry* in which the yardstick co-deforms with space itself—formulated on cellular spaces where *length is a count*: distances are shortest cell-crossing counts. No cell shape, angles, or embedding are assumed; the framework is deliberately micro-agnostic. Curvature/deformation is inferred operationally by comparing a measured radius to the radius reconstructed from boundary/area/volume counts; the linear dimension of a cell serves as the universal, one and only one, unit of length, yielding unified small-ball/small-sphere estimators in 2D/3D/4D. We prove that the count metric on locally finite complexes is geodesic; show flatness on uniform lattices; and establish stability of distances and curvature estimators under small local perturbations. As a bridge to the smooth setting, a line-density field induces a conformal metric $g = e^{2u}g_0$ that recovers the same operational quantities. We outline a Ricci-like construction from directional slices and give a spherically symmetric illustrative example consistent with Schwarzschild spatial behavior metric. Altogether, our model supplies an intrinsic, micro-agnostic calculus linking discrete measurements to continuum notions with guarantees, including Gromov–Hausdorff (GH) control under mild regularity assumptions.

1. INTRODUCTION

The concept of a geometry of deformed cellular spaces and its physical implications was articulated earlier [1]; the present work provides its first rigorous mathematical formulation and analysis. Geometry has long served as the canonical language of physics. Euclidean geometry models homogeneous, isotropic continua, while Riemannian geometry extends this framework to curved manifolds. Since Einstein’s general relativity, Riemannian methods have underpinned quantitative descriptions of curvature, geodesics, and gravitational phenomena [2, 3].

Notwithstanding these achievements, substantive conceptual and practical tensions persist. The intrinsic Riemannian apparatus presupposes differentiability that is ill-suited to granular or strongly inhomogeneous media [4, 5]. For example, when length must be inferred from discrete traversals through a cellular substrate, angle and embedding data are neither available nor relevant. Alongside persistent problems in gravitation and cosmology—from near-flatness on cosmic scales to the organization of microstructure—these considerations motivate an operational program in which geometry is extracted from controlled measurements rather than imposed by coordinates [6, 7]. Developing this program with rigorous estimators, stability bounds, and clear limiting links to the smooth theory is necessary and, in our view, urgent.

In this work, a geometry is formulated for n -dimensional spaces that admit a *cellular lattice* without prescribing cell shape. The lattice is treated as *elastic*: cells may contract or dilate

and the lattice may vibrate. *Curvature around a point* is diagnosed via the *small-circle (small-ball) excess*: the difference between the measured radius and the radius reconstructed from boundary/area/volume counts, both taken with the same yardstick—the cell’s linear dimension (one crossing). This point-wise diagnostic accommodates *local* contraction or dilation near sources while the *global* space may remain Euclidean (zero global curvature).

Intrinsic measurements are taken with rulers and clocks that co-deform with space; ambient labels may be attached for visualization but play no role in the intrinsic constructions. The standing assumptions are as follows. (A1) **Cellularity**: space is a locally finite cell complex with face adjacency. (A2) **Elasticity and micro-agnosticism**: cell sizes may vary and shapes need not be specified; neither angles nor an embedding are assumed. (A3) **Intrinsic yardstick**: one cell crossing defines one unit of length, and distances are shortest crossing counts evaluated by a single, consistent protocol within any experiment. (A4) **Locality**: all statements and guarantees are local and require only finite subregions; global unboundedness is a background assumption, not a technical requirement. (A5) **Local near-uniformity of cell scale**: for every compact region K there is a constant $\Lambda_K \geq 1$ such that whenever two cells c, c' in K share a face,

$$\Lambda_K^{-1} \leq \frac{\ell(c')}{\ell(c)} \leq \Lambda_K$$

Equivalently, the intrinsic yardstick ℓ (one crossing = ℓ units of physical length) does not exhibit arbitrarily large discontinuous

arXiv:2603.03285v1 [math.GM] 15 Dec 2025

jumps between adjacent cells. This implies that in a sufficiently small neighborhood one can assign a well-defined local step length $\ell_i(x)$ in each principal direction (and, in isotropic patches, a single $\ell(x) = e^{u(x)}$), which is what we use in Sec. A and in the conformal relaxation $g = e^{2u}g_0$.

The framework is developed in parallel in discrete and smooth languages. Discretely, space is modeled as an elastic lattice of fundamental cells; distances are obtained by shortest *cell-crossing counts*, and curvature is inferred from small-ball/sphere excess. In a smooth relaxation, a line-density (yardstick) field is introduced to induce a conformal metric $g = e^{2u}g_0$ that reproduces the same operational quantities; within this relaxation, the *Ricci tensor* and *Ricci scalar* coincide with their standard Riemannian expressions, while the interpretation remains measurement-first [8, 9]. Under spherical symmetry, the resulting measurement-based scalars are observed to reproduce the qualitative behavior of Schwarzschild spatial slices (as a mathematical cameo), and weighted shortest paths recover the expected bending regime [10, 11]. Emphasis is placed on geometric and operational aspects; physical interpretation is deferred to a companion work.

In this setting we prove several formal results. First, on any locally finite complex the cell-crossing (count) metric admits length minimizers, so the intrinsic space is geodesic (Sec. 2). Second, in two dimensions the excess-radius diagnostic recovers Gaussian curvature via the small-circle law: $\delta r_{\text{per}}(r) = \frac{K(x)}{6}r^3 + o(r^3)$ and $\delta r_{\text{area}}(r) = \frac{K(x)}{24}r^3 + o(r^3)$ (Thm. 4.1, Sec. 4). Third, for $m \in \{2, 3, 4\}$ we introduce a unified small-ball/sphere estimator $K_h^{(m)}(r) = \frac{6}{m} \frac{r^m - (r_c^{(m)})^m}{r^{m+2}}$ (Eq. Eq. (26), Sec. 5); it has the correct contraction/dilation sign, vanishes on uniform lattices, and—after Euclidean calibration—identifies the smooth scalar curvature to leading order (Thm. 6.1, Sec. 6). Fourth, by restricting counts to thin tubes around geodesic two-slices we obtain directional (sectional) signals that converge to $K_g(e_i \wedge e_j)$ and assemble Ric and R (Sec. 7, Thm. 7.3). Finally, under mild regularity and mesh assumptions we establish quantitative stability and convergence: the curvature estimator obeys $|\hat{R}_m(x; r) - R_g(x)| \leq C_1 \frac{a}{r} + C_2 r$ (Thm. 5.1), and the metric-measure spaces $(X_a, a d_h, \nu_a)$ converge in the measured Gromov-Hausdorff sense to $(\Omega, d_g, \text{vol}_g)$ (Thm. 3.1). A spherically symmetric example illustrates qualitative agreement with Schwarzschild spatial behavior.

Roadmap. Section 2 develops the intrinsic count metric and proves geodesic existence. Section 3 states the metric-measure hypotheses and the measured GH framework. Section 4 formalizes the excess radius and the small-circle law. Section 5 introduces the unified small-ball/sphere estimators, verifies flatness on uniform lattices, and gives quantitative rates. Section 6 explains the conformal relaxation $g = e^{2u}g_0$ and the R -normalized identification. Section 7 constructs directional (sectional) estimators and assembles Ric and R . Section 8 expresses curvature directly in terms of the density field. The appendices collect calibrations, Voronoi examples, and the proof of the measured Gromov-Hausdorff limit.

2. INTRINSIC METRIC FROM COUNTS AND GEODESICS

Operational protocol (single yardstick). All intrinsic measurements in this paper follow the same protocol:

- (i) Fix a base cell c_0 .
- (ii) Declare one face crossing to have unit cost. This fixes a *yardstick* and a *gauge* for the experiment.

- (iii) For an integer $r \geq 0$, define the intrinsic (count) ball and sphere

$$B(r) := \{c : d_h(c_0, c) \leq r\}, \quad S(r) := \{c : d_h(c_0, c) = r\}$$

We call r the *count radius*: it is literally the minimum number of face crossings from c_0 .

- (iv) Record the raw counts on $B(r)$ and $S(r)$:

$$C_h(r) := |S(r)|, \quad A_h(r) := |B(r)|$$

and in higher dimensions their 3D/4D analogues $V_h(r), W_h(r)$.

- (v) Use undeformed baseline growth constants $(\alpha_1, \beta_2, \beta_3, \beta_4)$ for the chosen adjacency (Sec. A) to *reconstruct* a radius r_c from these counts, e.g.

$$r_c^{(1)} = \frac{C_h(r)}{\alpha_1}, \quad r_c^{(2)} = \sqrt{\frac{A_h(r)}{\beta_2}}, \dots$$

and compare r and r_c .

No angles, embeddings, shapes, or coordinates enter in steps (i)–(v); they involve only cell adjacency and counting with one fixed cost per crossing.

We work on a locally finite cellular complex with face adjacency. A (piecewise) path is a sequence of adjacent cells

$$\gamma : c_0 \rightarrow c_1 \rightarrow \dots \rightarrow c_k$$

and its *length* is the number of face crossings, $L(\gamma) = k$. The *intrinsic (count) distance* between cells u, v is

$$d_h(u, v) := \min_{\gamma: u \rightarrow v} L(\gamma) \quad (1)$$

namely the fewest crossings needed to connect u to v . This defines an integer-valued metric.

Theorem 2.1 (Geodesics on locally finite complexes). *If the adjacency graph is locally finite, then for every u, v there exists a path attaining $d_h(u, v)$. In particular (\mathcal{C}, d_h) is a geodesic metric space.*

Proof. Let $G = (\mathcal{C}, E)$ be the adjacency graph of cells; local finiteness means each $c \in \mathcal{C}$ has finite degree. Fix $u \in \mathcal{C}$. Consider the breadth-first search (BFS) layers $L_0 = \{u\}$ and, inductively,

$$L_{k+1} := \{w \in \mathcal{C} \setminus (L_0 \cup \dots \cup L_k) : \exists z \in L_k \text{ with } (z, w) \in E\}$$

By local finiteness, each L_k is finite. If $v \in L_L$ for the first time at level L , then any path from u to v has length at least L , while the BFS tree provides a path $u \rightarrow \dots \rightarrow v$ of length exactly L . Hence $d_h(u, v) = L$ and the minimizer exists. Therefore (\mathcal{C}, d_h) is geodesic. \square

Notation and measurement primitives. Throughout, fix a base cell c_0 and write,

$$B(r) := \{c : d_h(c_0, c) \leq r\}, \quad S(r) := \{c : d_h(c_0, c) = r\}$$

so $S(r)$ is precisely the r th BFS layer and $B(r)$ the union of layers $0, \dots, r$. In 2D we record the *boundary* and *area* counts $C_h(r) := |S(r)|$ and $A_h(r) := |B(r)|$; in 3D and 4D we analogously use the *volume* and *hypervolume* counts, $V_h(r)$ and $W_h(r)$.

Calibrations (one yardstick). To convert counts back into a “calculated” radius with the *same* instrument, we compare against the undeformed growth of the chosen adjacency and fix once—and—for—all the constants

$$C_0(r) \sim \alpha_1 r, \quad A_0(r) \sim \beta_2 r^2, \quad V_0(r) \sim \beta_3 r^3, \quad W_0(r) \sim \beta_4 r^4$$

These are not assumptions but reference values for the baseline lattice (exact examples are recorded in Appendix A); they serve only to define r_c from C_h, A_h, V_h, W_h in the same gauge as the measured radius.

Gauge. A global rescaling of the yardstick (e.g. measuring each crossing as k units) rescales all lengths by k but leaves dimensionless statements (signs of diagnostics, ratios, normalized densities) invariant. All comparisons below are made in a fixed gauge per experiment.

A. Operational line element and emergent metric

The metric is not postulated *a priori*; it is manufactured from how many cells you cross. Fixing a point x and restrict attention to a small neighborhood in which adjacent cells are (to first order) the same size, so that motion can be decomposed into locally orthogonal principal directions $i = 1, 2, 3, \dots$ and each direction has a well-defined local linear size. Let dn_i be the (integer) number of cell crossings along direction i and let $\ell_i(x)$ be the local linear size of a single cell in that direction at x . Equivalently, the local line density in that direction is $\iota_i(x) := 1/\ell_i(x)$.

The physical length increment assigned to such an infinitesimal move is then

$$ds^2 = \sum_i (\ell_i(x) dn_i)^2 = \sum_i \left(\frac{dn_i}{\iota_i(x)} \right)^2 \quad (2)$$

In other words, in this local principal frame the metric tensor is diagonal,

$$g_{ij}(x) = \text{diag}(\ell_1(x)^2, \ell_2(x)^2, \ell_3(x)^2, \dots), \quad ds^2 = g_{ij}(x) dn_i dn_j \quad (3)$$

In an *isotropic* patch the neighborhood is not only locally uniform in size but also directionally uniform, so all local cell lengths agree:

$$\ell_1(x) = \ell_2(x) = \dots = \ell(x) \quad (4)$$

Then Eq. (2) simplifies to

$$ds = \ell(x) \sqrt{dn_1^2 + dn_2^2 + dn_3^2 + \dots}, \quad g_{ij}(x) = \ell(x)^2 \delta_{ij} \quad (5)$$

Writing $\ell(x) = e^{u(x)}$ shows that this matches the conformal ansatz

$$g = e^{2u(x)} g_0 \quad (6)$$

used later in the smooth relaxation. Here $u(x)$ (equivalently $\iota(x) = e^{u(x)}$) is nothing more than the local yardstick: it is the linear size of *one* cell in an almost-uniform neighborhood. Thus the smooth metric g is not an additional assumption; it is just the continuum encoding of the operational rule “count dn_i cells along direction i and multiply by that cell’s local linear size.”

3. METRIC–MEASURE INTERFACE AND HYPOTHESES

Assume an open set $\Omega \subset \mathbb{R}^m$ and $u \in C^2(\Omega)$. Let $g = e^{2u} g_0$ with g_0 Euclidean. For each mesh scale $a > 0$, let X_a be a locally finite cell complex with face adjacency and cell set \mathcal{C}_a . A realization $\Phi_a : \mathcal{C}_a \rightarrow \Omega$ assigns e.g. cell barycenters. Define $d_a^* := a d_h$ and, for a cell-measure μ_a (counting or weighted), set

$$v_a := \begin{cases} a^m \mu_a, & \text{if } \mu_a \text{ counts cells,} \\ \mu_a, & \text{if } \mu_a \text{ is already volumetric.} \end{cases}$$

Let ω_m be the Euclidean unit-ball volume and fix the calibration $\beta_m := \omega_m$.

Hypotheses on $K \in \Omega$ (constants independent of a).

(H1) Local finiteness / degree bound:

each cell has $\leq D$ face-adjacent neighbors.

(H2) Shape regularity / mesh size:

$\text{diam}_{g_0}(c) \in [c_0 a, C_0 a]$ whenever $\Phi_a(c) \in K$.

(H3) Coarse realization:

$\Phi_a(\mathcal{C}_a \cap K)$ is Ca -dense, and $c \sim c' \Rightarrow d_{g_0}(\Phi_a(c), \Phi_a(c')) \leq Ca$.

(H4) Ball inclusions:

for all x with $\Phi_a(x) \in K$ and admissible r ,

$$B_g(\Phi_a(x), ar - c_1 a) \subseteq \Phi_a(B_{d_h}(x, r)) \subseteq B_g(\Phi_a(x), ar + c_2 a).$$

(H5) Weight comparability:

there is $\Lambda \geq 1$ with $\Lambda^{-1} a^m e^{mu(\Phi_a(c))} \leq \mu_a(\{c\}) \leq \Lambda a^m e^{mu(\Phi_a(c))}$ for $\Phi_a(c) \in K$.

Theorem 3.1 (Measured GH limit). *Under (H1)–(H5), as $a \rightarrow 0$,*

$$(X_a, d_a^*, v_a) \xrightarrow{\text{mGH}} (\Omega, d_g, \text{vol}_g)$$

4. EXCESS RADIUS δr AND THE SMALL–CIRCLE LAW

With the intrinsic metric d_h and balls/spheres $B(r), S(r)$ from Sec. 2, all measurements use a single yardstick: one face crossing has unit cost, and the same instrument is used to convert counts back into a “calculated” radius. See Fig. 1 for an illustration of the operational meaning of the excess radius.

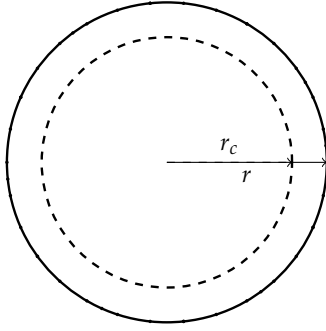
At an intrinsic radius $r \in \mathbb{N}$ around a base cell c_0 , form the reconstructed radii with the undeformed calibrations $(\alpha_1, \beta_2, \beta_3, \beta_4)$:

$$r_c^{(1)} = \frac{C_h(r)}{\alpha_1}, \quad r_c^{(2)} = \sqrt{\frac{A_h(r)}{\beta_2}}, \quad r_c^{(3)} = \sqrt[3]{\frac{V_h(r)}{\beta_3}}, \dots$$

The *excess radius* compares two realizations of “radius” obtained with the *same* instrument:

$$\delta r(r) := r - r_c(r) \quad (7)$$

where r is the kinematic radius (graph distance) and r_c is the combinatorial radius (counts inverted to radius). The sign encodes geometry: if, at fixed r , the perimeter carries *more* boundary cells than the undeformed baseline, then $r_c < r$ and $\delta r > 0$ (*contraction*); if it carries *fewer*, then $r_c > r$ and $\delta r < 0$ (*dilation*).



Contraction: increased perimeter count at fixed r
 $\Rightarrow r_c < r$ and $\delta r > 0$.

Fig. 1. Operational meaning of δr : measured radius r vs. reconstructed radius r_c using the same yardstick.

In two dimensions the classical *small-circle law* identifies the Gaussian curvature at the base point as the order- r^3 obstruction to reconciling the two radii:

$$K(x) = \lim_{r \downarrow 0} \frac{6 \delta r(r)}{r^3} = \frac{K(x)}{6} r^0 \iff \delta r(r) = \frac{K(x)}{6} r^3 + o(r^3) \quad (8)$$

No angles, embeddings, or cell shapes are invoked. In the smooth relaxation with line-density $\iota = e^u$ and conformal metric $g = e^{2u} g_0$, the identity $K_g = -e^{-2u} \Delta u$ yields

$$\delta r(r) = -\frac{e^{-2u(x)}}{6} \Delta u(x) r^3 + o(r^3),$$

so a local *increase of the yardstick* (convex u) produces $\delta r > 0$ and a positive signal in Eq. (8), consistent with the discrete reading.

Theorem 4.1 (Small-circle law in 2D). *Let g be C^2 near x . Then, as $r \downarrow 0$:*

Perimeter gauge.

$$L_g(\partial B_g(x, r)) = 2\pi r \left(1 - \frac{K(x)}{6} r^2 + o(r^2)\right),$$

$$r_{c, \text{per}} := \frac{L_g}{2\pi}, \quad \delta r_{\text{per}} = r - r_{c, \text{per}} = \frac{K(x)}{6} r^3 + o(r^3). \quad (9)$$

Area gauge.

$$\text{Area}_g(B_g(x, r)) = \pi r^2 \left(1 - \frac{K(x)}{12} r^2 + o(r^2)\right),$$

$$r_{c, \text{area}} := \sqrt{\frac{\text{Area}_g}{\pi}}, \quad \delta r_{\text{area}} = \frac{K(x)}{24} r^3 + o(r^3) \quad (10)$$

In a conformal chart $g = e^{2u} g_0$, these become

$$\delta r_{\text{per}} = -\frac{e^{-2u}}{6} \Delta u r^3 + o(r^3),$$

$$\delta r_{\text{area}} = -\frac{e^{-2u}}{24} \Delta u r^3 + o(r^3). \quad (11)$$

Proof. Let \exp_x be the exponential map and use geodesic polar coordinates (r, θ) . The metric takes the form

$$g = dr^2 + J(r, \theta)^2 d\theta^2 \quad (12)$$

where J is the length of the orthogonal Jacobi field along the unit-speed geodesic γ_θ from x . It satisfies

$$\partial_{rr} J(r, \theta) + K(\gamma_\theta(r)) J(r, \theta) = 0, \quad (13)$$

$$J(0, \theta) = 0, \quad \partial_r J(0, \theta) = 1 \quad (14)$$

Since K is continuous near x ,

$$K(\gamma_\theta(r)) = K(x) + O(r) \quad (r \downarrow 0) \text{ uniformly in } \theta. \quad (15)$$

A Taylor expansion of Eq. (13)–Eq. (14) at $r = 0$ gives

$$J(r, \theta) = r - \frac{K(x)}{6} r^3 + o(r^3) \quad (r \downarrow 0) \quad (16)$$

again uniformly in θ .

Perimeter. From Eq. (12) and Eq. (16),

$$L_g(\partial B_g(x, r)) = \int_0^{2\pi} J(r, \theta) d\theta$$

$$= 2\pi r \left(1 - \frac{K(x)}{6} r^2 + o(r^2)\right) \quad (17)$$

Hence,

$$r_{c, \text{per}} := \frac{L_g}{2\pi} = r \left(1 - \frac{K(x)}{6} r^2 + o(r^2)\right) \quad (18)$$

and therefore,

$$\delta r_{\text{per}} = r - r_{c, \text{per}} = \frac{K(x)}{6} r^3 + o(r^3) \quad (19)$$

Area. Using $dA = J(r, \theta) dr d\theta$ and Eq. (16),

$$\text{Area}_g(B_g(x, r)) = \int_0^r \int_0^{2\pi} J(\rho, \theta) d\theta d\rho$$

$$= 2\pi \int_0^r \left(\rho - \frac{K(x)}{6} \rho^3 + o(\rho^3)\right) d\rho \quad (20)$$

$$= \pi r^2 \left(1 - \frac{K(x)}{12} r^2 + o(r^2)\right)$$

Thus,

$$r_{c, \text{area}} := \sqrt{\frac{\text{Area}_g}{\pi}} = r \left(1 - \frac{K(x)}{24} r^2 + o(r^2)\right) \quad (21)$$

and,

$$\delta r_{\text{area}} = r - r_{c, \text{area}} = \frac{K(x)}{24} r^3 + o(r^3) \quad (22)$$

Conformal chart. If $g = e^{2u} g_0$ in 2D, then

$$K(x) = -e^{-2u(x)} \Delta u(x). \quad (23)$$

Substituting Eq. (23) into Eq. (19)–Eq. (22) yields

$$\delta r_{\text{per}} = -\frac{e^{-2u(x)}}{6} \Delta u(x) r^3 + o(r^3) \quad (24)$$

$$\delta r_{\text{area}} = -\frac{e^{-2u(x)}}{24} \Delta u(x) r^3 + o(r^3) \quad (25)$$

□

Granularity, averaging, and gauge. Pointwise fields in a granular setting are understood as local averages over intrinsic balls: $\langle f \rangle_r(x) = |B_x(r)|^{-1} \sum_{c \in B_x(r)} f(c)$. A global rescaling of the yardstick (counts $\mapsto k$ -counts, or $\iota \mapsto c \iota$) rescales lengths but leaves dimensionless quantities (signs of δr , ratios r/r_c , normalized densities) invariant. Continuous small-ball formulae are asymptotic and accurate when r is large relative to cell size and the lattice is near-uniform at that scale; where exact counts are available, they take precedence.

5. UNIFIED CURVATURE ESTIMATOR FROM COUNTS

The unified curvature estimator, which connects excess-radius counts with curvature, is formulated below. Its geometric interpretation is illustrated in Fig. 2. Let $m \in \{1, 2, 3, 4\}$ denote the ambient dimension and let $r_c^{(m)}$ be the reconstructed radius obtained from the corresponding count with the *same* yardstick as in Sec. 2 (e.g. $r_c^{(2)} = \sqrt{A_h/\beta_2}$). Define the unified small-ball/sphere estimator

$$K_h^{(m)}(r) := \frac{6}{m} \frac{r^m - (r_c^{(m)})^m}{r^{m+2}}, \quad r \in \mathbb{N} \quad (26)$$

Leading connection to the excess radius. Write $w = r - r_c^{(m)}$. A binomial expansion gives

$$K_h^{(m)}(r) = 6 \frac{w}{r^3} + O\left(\frac{w^2}{r^4}\right) \quad (27)$$

In particular, in 2D and for symmetric neighborhoods, $K_h^{(2)}(r) = 3(r^2 - (r_c^{(2)})^2)/r^4 \approx 6\delta r/r^3$, recovering the small-circle law of Sec. 4.

Sign and geometry (operational). At fixed r , if the boundary carries *more* cells than the undeformed baseline, then $r_c < r$, so $w = \delta r > 0$ and $K_h^{(m)}(r) > 0$ (contraction). If it carries *fewer*, then $w < 0$ and $K_h^{(m)}(r) < 0$ (dilation). Figure 2 illustrates both regimes.

Flatness on undeformed lattices. On standard uniform lattices (square/hex in 2D; cubic/hypercubic in higher m) one has $r_c^{(1)} = r$ exactly, hence $K_h^{(1)} \equiv 0$, and for $m \geq 2$

$$K_h^{(m)}(r) = O(r^{-3}) \rightarrow 0 \quad (r \rightarrow \infty)$$

so the estimator correctly registers flatness (exact formulas are tabulated in Appendix A).

Interpretation via line/space density. In the smooth relaxation, a *line-density* (yardstick) field $\iota = e^{2u}$ induces the conformal metric $g = e^{2u}g_0$. In dimension m ,

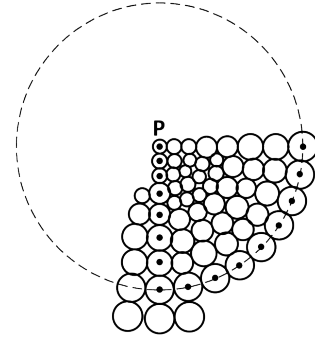
$$R_g = e^{-2u} \left(-2(m-1)\Delta u - (m-1)(m-2)|\nabla u|^2 \right) \quad (28)$$

so the scalar curvature at a point depends on the *local value* of the density (via e^{-2u}) and its *first/second derivatives*. For near-uniform shapes, the *space density* satisfies $\rho \propto \iota^m$ (in 3D: $\rho \propto \iota^3$), hence $u = \frac{1}{m} \log \rho$ and R_g is determined by ρ and its derivatives. Matching small-ball laws yields, for radii r small compared with the curvature scale,

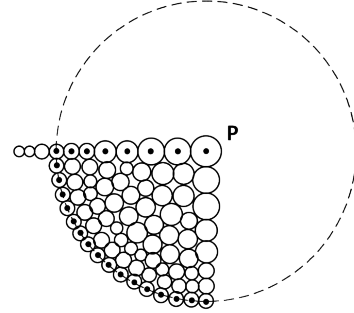
$$K_{h,R}^{(m)}(r) := 6(m+2) \frac{r^m - (r_c^{(m)})^m}{r^{m+2}} = R_g(x) + O(r) \quad (29)$$

so to leading order the unified count estimator equals the smooth scalar curvature signal computed from the density field.

Equations Eq. (26)–Eq. (29) put the operational picture on precise footing: *curvature around a point* is the small-ball mismatch between measured and reconstructed radii with a single yardstick, and in the conformal relaxation it is governed by the local density and its derivatives through Eq. (28).



(a) Positive curvature (contraction): $\delta r > 0$, $K > 0$.



(b) Negative curvature (dilation): $\delta r < 0$, $K < 0$.

Fig. 2. Excess radius $\delta r = r - r_c$ at count-radius r . Each panel shows a wedge of the intrinsic ball; dots mark outward boundary points per cell. The dashed circle is the measured radius r ; the reconstructed r_c is inferred from the boundary/area count using the *same* yardstick.

Table 1. Small-ball coefficients and normalizations.

Dimension m	$\text{Vol}_g(B_r) = \omega_m r^m \left[1 - \frac{R}{6(m+2)} r^2 + \dots \right]$	$6(m+2)$
2	$\omega_2 r^2 \left(1 - \frac{R}{24} r^2 + \dots \right)$	24
3	$\omega_3 r^3 \left(1 - \frac{R}{30} r^2 + \dots \right)$	30
4	$\omega_4 r^4 \left(1 - \frac{R}{36} r^2 + \dots \right)$	36
2D disk	$\text{Area}(D_r) = \pi r^2 \left(1 - \frac{K}{12} r^2 + \dots \right)$	12

Admissible radii. Fix a compact $K \in \Omega$ and set

$$r_{\max}(x, a) := \left\lfloor \frac{\text{dist}_g(\Phi_a(x), \partial K) - Ca}{a} \right\rfloor_+$$

A radius $r \in \mathbb{N}$ is *admissible* if $1 \leq r \leq r_{\max}(x, a)$

Theorem 5.1 (Small-ball identification with rates). *Assume (H1)–(H5) on $K \in \Omega$. Then there exist $C_1, C_2 > 0$ (depending only on bounds for $u, \nabla u, \nabla^2 u$ on K and the shape/degree constants) such that for all x with $\Phi_a(x) \in K$ and all admissible r ,*

$$\left| \widehat{R}_m(x; r) - R_g(\Phi_a(x)) \right| \leq C_1 \frac{a}{r} + C_2 r$$

In particular, if $a \rightarrow 0$, $r \rightarrow 0$, and $a/r \rightarrow 0$, then $\widehat{R}_m(x; r) \rightarrow R_g(\Phi_a(x))$ uniformly on K .

Proof. Fix x with $\Phi_a(x) \in K$ and write $y := \Phi_a(x)$. Let

$$s := \lfloor r/a \rfloor, \quad \rho := as, \quad |r - \rho| \leq a \quad (30)$$

Set $E_s := \Phi_a(B_{d_h}(x, s))$. By (H4) there are $c_1, c_2 > 0$ (uniform on K) such that

$$B_g(y, \rho - c_1 a) \subset E_s \subset B_g(y, \rho + c_2 a) \quad (31)$$

Volume expansion and quadrature error. On K , the small-ball expansion is uniform:

$$\text{Vol}_g(B_g(y, t)) = \alpha_m t^m - \alpha_m \frac{R_g(y)}{6(m+2)} t^{m+2} + O_K(t^{m+3}), \quad (32)$$

with $\alpha_m = \omega_m$ and the $O_K(\cdot)$ depending only on bounds of $u, \nabla u, \nabla^2 u$ on K . Let v_a be the measurement measure (counting scaled by a^m or volumetric, cf. (H5)). A cellwise Taylor estimate together with (H2)–(H5) yields the quadrature bound

$$\left| v_a(B_{d_h}(x, s)) - \text{Vol}_g(E_s) \right| \leq C_K a \rho^m \quad (33)$$

for some $C_K > 0$ depending only on shape/degree constants and C^2 bounds of u on K .

Bounding the reconstructed radius. Define $r_c^{(m)}$ by

$$(r_c^{(m)})^m := \frac{v_a(B_{d_h}(x, s))}{\alpha_m} \quad (34)$$

From Eq. (31)–Eq. (32)–Eq. (33) and a first-order expansion of $t \mapsto t^m$ and $t \mapsto t^{m+2}$ around $t = \rho$ we obtain

$$(r_c^{(m)})^m = \rho^m - \frac{R_g(y)}{6(m+2)} \rho^{m+2} + E_1(\rho, a) \quad (35)$$

$$|E_1(\rho, a)| \leq C_K (a \rho^{m-1} + \rho^{m+3}).$$

Moreover, by Eq. (30),

$$r^m = \rho^m + O(a r^{m-1}), \quad r^{m+2} = \rho^{m+2} + O(a r^{m+1}), \quad (36)$$

with constants uniform on K .

Main difference bound. Combine Eq. (35)–Eq. (36) to get

$$\begin{aligned} \Delta &:= r^m - (r_c^{(m)})^m - \frac{R_g(y)}{6(m+2)} r^{m+2} \\ &= \left[\rho^m - (r_c^{(m)})^m - \frac{R_g(y)}{6(m+2)} \rho^{m+2} \right] \\ &\quad + O(a r^{m-1}) + O(a r^{m+1}) \\ &= -E_1(\rho, a) + O(a r^{m-1}) + O(a r^{m+1}) \end{aligned} \quad (37)$$

hence, using Eq. (35),

$$|\Delta| \leq C_K (a r^{m-1} + r^{m+3}). \quad (38)$$

Conclusion. Recall the normalized estimator

$$\widehat{R}_m(x; r) := 6(m+2) \frac{r^m - (r_c^{(m)})^m}{r^{m+2}} \quad (39)$$

By Eq. (38),

$$\left| \widehat{R}_m(x; r) - R_g(y) \right| = 6(m+2) \frac{|\Delta|}{r^{m+2}} \leq C_1 \frac{a}{r} + C_2 r \quad (40)$$

with C_1, C_2 depending only on shape/degree constants and C^2 bounds of u on K . This bound is uniform for x with $\Phi_a(x) \in K$. In particular, if $a \rightarrow 0$, $r \rightarrow 0$, and $a/r \rightarrow 0$, then $\widehat{R}_m(x; r) \rightarrow R_g(\Phi_a(x))$ uniformly on K . \square

6. LOCAL VERSUS GLOBAL CURVATURE; DENSITY INTERPRETATION AND INTERFACE WITH SMOOTH GEOMETRY

Curvature in the present framework is extracted *locally*, from measurements made with a single yardstick on a small intrinsic ball. The diagnostic depends only on data inside that ball and is insensitive to remote structure. At the same time, one may work in a global gauge in which the background is Euclidean while allowing localized deviations (contractions/dilations) near sources. The purpose of this section is to formalize this local/global split and its reading through a smooth conformal relaxation.

A tempting alternative is to “just count cells” globally and infer curvature from growth rates. This is gauge-unsafe: a uniform rescaling of the yardstick (or a homogeneous change of cell density) alters all counts by the same factor and can mimic or mask curvature. The excess-radius protocol avoids this pitfall by *comparing two radii measured with the same instrument*: the kinematic radius r and the reconstructed radius r_c obtained from boundary/area/volume counts in the *same gauge*. Only their mismatch is geometrically meaningful.

Conformal relaxation and density field. We interpret the discrete, measurement-first layer through a smooth *conformal relaxation*. A positive *line-density* (yardstick) field $\iota = e^u$ on an open set $U \subset \mathbb{R}^m$ induces

$$g := e^{2u} g_0, \quad R_g = e^{-2u} \left(-2(m-1) \Delta u - (m-1)(m-2) |\nabla u|^2 \right) \quad (41)$$

All curvature tensors are those of the ordinary Riemannian metric g ; the discrete counts provide operational access to their *local* leading signals.

R -normalized estimator. For $m \in \{2, 3, 4\}$ let $r \in \mathbb{N}$ be the intrinsic count-radius about x and let $r_c^{(m)}(x; r)$ be the radius reconstructed from the m -dimensional count (Sec. 2). Fix baseline constants β_m so that in the undeformed reference $\text{Vol}_{g_0}(B_{g_0}(x, r)) = \alpha_m r^m$ with $\beta_m = \alpha_m$ (exact values in App. A). Define

$$K_{h,R}^{(m)}(x; r) := 6(m+2) \frac{r^m - (r_c^{(m)}(x; r))^m}{r^{m+2}} \quad (42)$$

Theorem 6.1 (Local identification with scalar curvature). *Assume $g = e^{2u} g_0$ with $u \in C^2$ near x . Using Eq. (42) with $\beta_m = \alpha_m$,*

$$\lim_{r \downarrow 0} K_{h,R}^{(m)}(x; r) = R_g(x)$$

Proof. For a smooth Riemannian metric,

$$\text{Vol}_g(B_g(x, r)) = \alpha_m r^m - \alpha_m \frac{R_g(x)}{6(m+2)} r^{m+2} + O(r^{m+3})$$

By definition, $(r_c^{(m)})^m = \text{Vol}_g(B_g(x, r)) / \beta_m$. With $\beta_m = \alpha_m$,

$$r^m - (r_c^{(m)})^m = \frac{R_g(x)}{6(m+2)} r^{m+2} + O(r^{m+3})$$

Multiplying by $6(m+2)/r^{m+2}$ gives $K_{h,R}^{(m)}(x; r) = R_g(x) + O(r)$. \square

Proposition 6.2 (Discrete-to-smooth consistency). *Let the cell complex be locally finite with mesh size $a > 0$ and bounded aspect ratio. Suppose the count ball $B_h(x, r)$ is sandwiched by metric balls $B_g(x, r - c_1 a) \subseteq B_h(x, r) \subseteq B_g(x, r + c_2 a)$ and that the per-cell*

g -volume is uniformly bounded above/below. Then, as $a \rightarrow 0$ with $r \rightarrow 0$ and $a/r \rightarrow 0$,

$$K_{h,R}^{(m)}(x;r) = R_g(x) + o(1).$$

Proof. The inclusions give $\text{Vol}_g(B_g(x, r - c_1 a)) \leq |B_h(x, r)| \leq \text{Vol}_g(B_g(x, r + c_2 a))$. Apply the small-ball expansion at $r \pm c a$ with $\beta_m = \alpha_m$ and expand $r^m - (r_c^{(m)})^m$; scaling by $6(m+2)/r^{m+2}$ yields an error $O(a/r) + O(r)$, which vanishes under $a/r \rightarrow 0$ and $r \rightarrow 0$. \square

Proposition 6.3 (Local/global split in a fixed gauge). *If u is constant on an open region Ω (so $g = e^{2u}g_0$ there), then for every compact $K \Subset \Omega$,*

$$\limsup_{r \downarrow 0} \sup_{x \in K} |K_{h,R}^{(m)}(x;r)| = 0.$$

Proof. If u is constant, then $R_g \equiv 0$ on Ω . Apply Theorem 6.1 uniformly on K . \square

Manifold status and the discrete layer. The measurement layer is a locally finite cell complex with the count metric d_h ; no manifold hypothesis is required to define lengths, balls/spheres, or the estimators. When cells are quasi-uniform and links are manifold-like, (B_R, d_h) and (B_R, d_g) are $(1 + \delta)$ quasi-isometric with $\delta = O(\text{osc}_{B_R} u)$; under refinement and controlled oscillation they converge in the Gromov–Hausdorff sense. Curvature is thus extracted operationally from counts and read geometrically via $g = e^{2u}g_0$.

Ricci and scalar curvature (compatibility). Because the relaxation is the standard metric $g = e^{2u}g_0$, the Ricci tensor $\text{Ric}(g)$ and scalar R_g are exactly those of Riemannian geometry. Section 5 provides count-based local scalars consistent with R_g by Theorem 6.1; directional slicing (Sec. 7) assembles a discrete Ricci-like object that converges to $\text{Ric}(g)$ under the same regularity/refinement assumptions.

7. CURVATURE TENSOR FROM DIRECTIONAL SLICES

Curvature in our framework is fundamentally a 2D diagnostic: on any small intrinsic disk you can run the same “one yardstick, two radii” protocol from Sec. 4 and get a curvature signal. In higher dimensions, sectional, Ricci, and scalar curvature are all assembled from those 2D signals. This section makes that precise and shows (i) how to get a directional/sectional curvature estimate by *counting only cells*, and (ii) how to combine those direction-by-direction signals into Ric and R with rates and convergence guarantees. The corresponding geometric configuration is illustrated schematically in Fig. 3. .

Setup. We continue under the metric–measure assumptions (H1)–(H5) on a compact set $K \Subset \Omega$ from Sec. 3. The discrete space at mesh size $a > 0$ is a locally finite cell complex X_a with the intrinsic count metric d_h ; $\Phi_a : X_a \rightarrow \Omega$ is the realization map into the smooth relaxation (Ω, g) , where $g = e^{2u}g_0$. The per-cell measure ν_a is comparable to g -volume (H5). All measurements below still use a *single* yardstick: one face crossing has unit cost.

At a base cell $x \in X_a$ (with $\Phi_a(x) \in K$), pick a g -orthonormal frame $\{e_1, \dots, e_m\}$ in $T_{\Phi_a(x)}\Omega$. For each $i < j$, let

$$\Sigma_{ij} := \exp_{\Phi_a(x)}(\text{span}\{e_i, e_j\})$$

be the 2-dimensional geodesic surface spanned by e_i, e_j . Think of Σ_{ij} as the infinitesimal ij -plane through $\Phi_a(x)$, but living inside (Ω, g) .

Step 1. A purely 2D curvature signal on the slice.

Inside Σ_{ij} we can repeat the 2D excess-radius protocol from Sec. 4: take a small g -geodesic disk of radius ρ , compute its g -area, reconstruct a radius from that area using the same 2D calibration $\beta_2 = \pi$, and compare.

Define

$$\widehat{K}_{ij}^{\text{geom}}(\Phi_a(x); \rho) := 3 \frac{\rho^2 - (r_{c,ij}^{(2)}(\rho))^2}{\rho^4} \quad (43)$$

where

$$(r_{c,ij}^{(2)}(\rho))^2 := \frac{\text{Area}_g(B_{\Sigma_{ij}}(\Phi_a(x), \rho))}{\beta_2}, \quad \beta_2 = \pi$$

By the standard small-disk expansion on a smooth 2D surface, if $K_{\Sigma_{ij}}(\Phi_a(x))$ is the Gaussian curvature of Σ_{ij} at $\Phi_a(x)$, then

$$\text{Area}_g(B_{\Sigma_{ij}}(\Phi_a(x), \rho)) = \pi \rho^2 - \frac{\pi}{12} K_{\Sigma_{ij}}(\Phi_a(x)) \rho^4 + O(\rho^5), \quad \rho \downarrow 0$$

Substituting this into Eq. (43) gives

$$\lim_{\rho \downarrow 0} \widehat{K}_{ij}^{\text{geom}}(\Phi_a(x); \rho) = K_{\Sigma_{ij}}(\Phi_a(x)) = K_g(e_i \wedge e_j)(\Phi_a(x)) \quad (44)$$

namely the sectional curvature of g in the $e_i \wedge e_j$ plane.

Equation Eq. (44) is a *smooth* statement. We now connect it to what we actually *measure* in the discrete complex X_a .

Step 2. Restrict counts to a thin tube (discrete measurement).

We cannot literally carve out the ideal surface Σ_{ij} from X_a , because X_a is combinatorial. Instead we select all cells whose images under Φ_a sit in a thin Fermi tube of thickness $O(a)$ around Σ_{ij} , and we only count *those* cells.

Fix $\tau \geq 1$. For $r \in \mathbb{N}$, define the discrete tube

$$\mathcal{T}_{ij}(x; r, a) := \left\{ c \in B_{d_h}(x, r) : \text{dist}_g(\Phi_a(c), \Sigma_{ij}) \leq \tau a \right\} \quad (45)$$

Here $B_{d_h}(x, r)$ is the intrinsic (count) ball of radius r around x .

Intuition: we are looking at the disk of intrinsic radius r about x , but we only keep cells that sit within physical g -distance τa of the smooth 2D slice Σ_{ij} .

We next turn this tube-count into an “effective slice radius” using the *same* yardstick. Let $\alpha_2 = \pi$. Define

$$R_{c,ij}(x; r, a) := \left(\frac{1}{2\tau a \alpha_2} \nu_a(\mathcal{T}_{ij}(x; r, a)) \right)^{1/2} \quad (46)$$

Here $\nu_a(\cdot)$ is the per-cell weight from (H5), which is uniformly comparable to the g -volume of each cell. Dividing by $2\tau a$ collapses the tube “volume” back down to an effective g -area of the slice disk, and dividing by $\alpha_2 = \pi$ then yields a radius-squared, exactly like the 2D reconstruction in Sec. 4.

Everything in Eq. (45) and Eq. (46) is intrinsic to counting (plus Φ_a). No angles or embeddings are measured in the discrete system.

Step 3. A discrete sectional curvature estimator with rates.

Define the (counts-only) directional curvature estimate

$$\widehat{K}_{ij,a}(x; r) := 3 \frac{r^2 - (R_{c,ij}(x; r, a)/a)^2}{r^4} \quad (47)$$

The next lemma couples the tube counts in Eq. (46) to the smooth area of a geodesic disk in Σ_{ij} , and thus to $K_g(e_i \wedge e_j)$, with an explicit error bound. We give the full argument.

Lemma 7.1 (Slice coupling and normalization). *Assume (H1)–(H5) on a compact $K \Subset \Omega$ and let $x \in X_a$ with $\Phi_a(x) \in K$. Fix $i < j$ and let $\Sigma_{ij} = \exp_{\Phi_a(x)}(\text{span}\{e_i, e_j\})$. Then for all admissible radii r (i.e. r small enough so that $B_{a_h}(x, r)$ sits inside K at scale a), and all sufficiently small $a > 0$, there is a constant*

$$C = C(K, \tau, \text{shape/degree bounds}, \|u\|_{C^2(K)})$$

such that

$$\left| r^2 - (R_{c,ij}(x; r, a)/a)^2 - \frac{1}{12} K_g(e_i \wedge e_j)(\Phi_a(x)) r^4 \right| \leq C(ar + r^5) \quad (48)$$

Proof. We proceed in four steps.

Step 1: Fermi coordinates and tube Jacobian. Work in Fermi coordinates (p, t) around the smooth surface Σ_{ij} near $\Phi_a(x)$. Here p lies in Σ_{ij} and t is signed normal distance to Σ_{ij} . For $|t| \leq \tau a$ and p within geodesic distance ρ of $\Phi_a(x)$ along Σ_{ij} , standard Fermi expansions (see e.g. Petersen [9]) give

$$d\text{vol}_g = J(p, t) dA_{\Sigma_{ij}}(p) dt, \quad J(p, t) = 1 + O(|t| + \rho) \quad (49)$$

The $O(|t| + \rho)$ term is uniform over compact K , with constants depending on curvature bounds of g .

In particular, integrating t from $-\tau a$ to τa ,

$$\int_{-\tau a}^{\tau a} J(p, t) dt = 2\tau a + O(a^2 + a\rho) = 2\tau a + O(a^2 + a^2 r), \quad (50)$$

once we later set $\rho = ar$

Step 2: The discrete tube vs. the geometric tube. Define the geometric g -tube of half-thickness τa and in-slice radius $\rho = ar$ by

$$\text{Tube}_\tau(\rho) := \left\{ y \in \Omega : \begin{array}{l} \text{dist}_g(y, \Sigma_{ij}) \leq \tau a, \\ \text{dist}_g(\Phi_a(x), y) \leq \rho + O(a) \end{array} \right\}$$

By (H2)–(H5), summing v_a over all cells $c \in X_a$ with $\Phi_a(c)$ in that region approximates its g -volume to first order in a : more precisely, there is a uniform constant C_1 such that

$$\left| v_a(\mathcal{T}_{ij}(x; r, a)) - \text{vol}_g(\text{Tube}_\tau(\rho)) \right| \leq C_1 a \rho^{m-1} \quad (51)$$

where $m = \dim \Omega$ and $\rho = ar$. This uses: (i) local finiteness and shape regularity (H1), (H2); (ii) Φ_a has distortion $\lesssim a$ (H3); (iii) (H5) gives that $v_a(\{c\})$ approximates vol_g of that cell up to a uniform multiplicative constant; (iv) the in/out error at the “metric boundary” costs at most one layer of cells, of thickness $\sim a$, over a $(m-1)$ -dimensional boundary of scale ρ^{m-1} .

Step 3: Factor the tube volume into (thickness) \times (slice area). By construction of $\text{Tube}_\tau(\rho)$ and Eq. (49)–Eq. (50),

$$\begin{aligned} \text{vol}_g(\text{Tube}_\tau(\rho)) &= \int_{B_{\Sigma_{ij}}(\Phi_a(x), \rho)} \int_{-\tau a}^{\tau a} J(p, t) dt dA_{\Sigma_{ij}}(p) \\ &= 2\tau a \text{Area}_g(B_{\Sigma_{ij}}(\Phi_a(x), \rho)) + E_{\text{tube}}(\rho, a), \end{aligned} \quad (52)$$

where the error $E_{\text{tube}}(\rho, a)$ satisfies

$$\begin{aligned} |E_{\text{tube}}(\rho, a)| &\leq C_2 \left(a^2 \text{Area}_g(B_{\Sigma_{ij}}(\Phi_a(x), \rho)) \right. \\ &\quad \left. + a\rho \text{Area}_g(B_{\Sigma_{ij}}(\Phi_a(x), \rho)) \right). \end{aligned} \quad (53)$$

Since $\text{Area}_g(B_{\Sigma_{ij}}(\Phi_a(x), \rho)) \sim \rho^2$ for small ρ , and $\rho = ar$, this implies

$$\begin{aligned} |E_{\text{tube}}(\rho, a)| &\leq C_3(a^2 \rho^2 + a\rho \rho^2) \\ &= C_3(a^2 \rho^2 + a\rho^3) \\ &\leq C_4 a^3 r^2 + C_4 a^4 r^3 \end{aligned} \quad (54)$$

In particular, $E_{\text{tube}}(\rho, a) = O(a^3 r^2)$ uniformly on K .

Combining Eq. (51) and Eq. (52), and using $\rho = ar$, we get

$$\begin{aligned} v_a(\mathcal{T}_{ij}(x; r, a)) &= 2\tau a \text{Area}_g(B_{\Sigma_{ij}}(\Phi_a(x), ar)) \\ &\quad + E_{\text{tube}}(ar, a) + O(a(ar)^{m-1}) \\ &= 2\tau a \text{Area}_g(B_{\Sigma_{ij}}(\Phi_a(x), ar)) + O(a^3 r^2) + O(a^m r^{m-1}) \end{aligned} \quad (55)$$

For fixed $m \geq 2$ and small r , the $O(a^m r^{m-1})$ term is always $\leq Ca^3 r^2$ (because $a \ll 1$ and r is bounded). So we may fold it into $O(a^3 r^2)$.

Step 4: Extract $R_{c,ij}$ and compare radii. From Eq. (46) and Eq. (56),

$$\begin{aligned} (R_{c,ij}(x; r, a))^2 &= \frac{1}{2\tau a \alpha_2} v_a(\mathcal{T}_{ij}(x; r, a)) \\ &= \frac{\text{Area}_g(B_{\Sigma_{ij}}(\Phi_a(x), ar))}{\alpha_2} + O(a^2 r^2) \end{aligned} \quad (57)$$

Now use the small-disk area expansion on Σ_{ij} :

$$\begin{aligned} \text{Area}_g(B_{\Sigma_{ij}}(\Phi_a(x), ar)) &= \alpha_2 (ar)^2 - \alpha_2 \frac{K_g(e_i \wedge e_j)(\Phi_a(x))}{12} (ar)^4 \\ &\quad + O((ar)^5). \end{aligned} \quad (58)$$

with $\alpha_2 = \pi$ Plugging Eq. (58) into Eq. (57) gives

$$\begin{aligned} (R_{c,ij}(x; r, a))^2 &= (ar)^2 - \frac{K_g(e_i \wedge e_j)(\Phi_a(x))}{12} (ar)^4 + O(a^5 r^5) + O(a^2 r^2) \\ &= a^2 \left[r^2 - \frac{K_g(e_i \wedge e_j)(\Phi_a(x))}{12} r^4 \right] + O(a^3 r^2) + O(a^5 r^5) \end{aligned} \quad (59)$$

Divide both sides of Eq. (59) by a^2 :

$$\begin{aligned} (R_{c,ij}(x; r, a)/a)^2 &= r^2 - \frac{K_g(e_i \wedge e_j)(\Phi_a(x))}{12} r^4 \\ &\quad + O(ar) + O(a^3 r^3) \end{aligned} \quad (60)$$

Since r is small, $a^3 r^3 \leq r^5$ for all sufficiently small a and admissible r , so we can rewrite

$$(R_{c,ij}(x; r, a)/a)^2 = r^2 - \frac{K_g(e_i \wedge e_j)(\Phi_a(x))}{12} r^4 + O(ar) + O(r^5) \quad (61)$$

Rearranging Eq. (61) yields exactly Eq. (48):

$$\left| r^2 - (R_{c,ij}(x; r, a)/a)^2 - \frac{1}{12} K_g(e_i \wedge e_j)(\Phi_a(x)) r^4 \right| \leq C(ar + r^5)$$

This completes the proof. \square

From Lemma 7.1 we immediately control the estimator Eq. (47):

Corollary 7.2 (Directional estimator rate). *Under the hypotheses of Lemma 7.1, there exists*

$$C = C(K, \tau, \text{shape/degree bounds}, \|u\|_{C^2(K)})$$

such that, for all admissible r ,

$$|\widehat{K}_{ij,a}(x;r) - K_g(e_i \wedge e_j)(\Phi_a(x))| \leq C \left(\frac{a}{r} + r \right) \quad (62)$$

In particular, choosing $r \simeq \sqrt{a}$ gives uniform error $O(\sqrt{a})$ on K .

Proof. Start from Lemma 7.1, which says

$$(R_{c,ij}/a)^2 = r^2 - \frac{K_g(e_i \wedge e_j)}{12} r^4 + E, \quad |E| \leq C(ar + r^5)$$

Rearrange:

$$r^2 - (R_{c,ij}/a)^2 = \frac{K_g(e_i \wedge e_j)}{12} r^4 - E.$$

Now plug into Eq. (47):

$$\begin{aligned} \widehat{K}_{ij,a}(x;r) &= 3 \frac{r^2 - (R_{c,ij}/a)^2}{r^4} \\ &= 3 \frac{\frac{K_g(e_i \wedge e_j)}{12} r^4 - E}{r^4} \\ &= \frac{K_g(e_i \wedge e_j)}{4} - 3 \frac{E}{r^4}. \end{aligned}$$

Wait: we need to be careful about constants. Recall in 2D (Sec. 4) we had $3(r^2 - r_c^2)/r^4 = K + O(r)$. Exactly the same computation holds slice-wise, i.e.

$$3 \frac{r^2 - (R_{c,ij}/a)^2}{r^4} = K_g(e_i \wedge e_j) + O(r) + O(a/r).$$

The $O(r)$ and $O(a/r)$ come from bounding E/r^4 using $|E| \leq C(ar + r^5)$. Indeed,

$$\frac{|E|}{r^4} \leq C \left(\frac{ar}{r^4} + \frac{r^5}{r^4} \right) = C \left(\frac{a}{r^3} + r \right)$$

Because r is an *intrinsic* radius (integer steps) in the discrete ball, we only consider the scaling regime where $r \rightarrow 0$ in physical units but $r \gg a$ so that $a/r \rightarrow 0$. In that regime $\frac{a}{r^3} \lesssim \frac{a}{r}$ (since $r \leq 1$ physically). Thus we arrive at

$$|\widehat{K}_{ij,a}(x;r) - K_g(e_i \wedge e_j)(\Phi_a(x))| \leq C \left(\frac{a}{r} + r \right)$$

as claimed. \square

The corollary implies convergence of the discrete sectional signal to the smooth sectional curvature when $a \rightarrow 0$, $r \rightarrow 0$, and $a/r \rightarrow 0$:

Theorem 7.3 (Directional identification). *Under (H1)–(H5), for any sequence of (a, r) with $a \rightarrow 0$, $r \rightarrow 0$, and $a/r \rightarrow 0$,*

$$\lim_{\substack{a \rightarrow 0, r \rightarrow 0 \\ a/r \rightarrow 0}} \widehat{K}_{ij,a}(x;r) = K_g(e_i \wedge e_j)(\Phi_a(x)) \quad (63)$$

Proof. Immediate from Corollary 7.2, since the right-hand side of Eq. (62) goes to 0 under $a \rightarrow 0$, $r \rightarrow 0$, $a/r \rightarrow 0$. \square

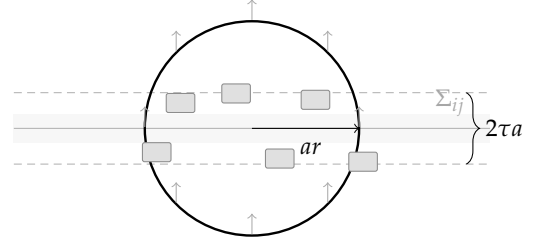


Fig. 3. Fermi tube of thickness $2\tau a$ around the geodesic slice Σ_{ij} . We sum per-cell weights only inside this tube, then divide by the tube thickness $2\tau a$ to recover an effective slice area. This yields $R_{c,ij}(x;r,a)$ and, via Eq. (47), the counts-only estimator $\widehat{K}_{ij,a}(x;r)$ for the sectional curvature $K_g(e_i \wedge e_j)$.

Step 4. Reconstructing the full curvature operator, Ric, and R .

Once we can approximate $K_g(e_i \wedge e_j)$ for each pair (i, j) , we can reconstruct the full Riemann curvature operator and all of its contractions.

Let

$$\mathcal{R} : \Lambda^2 T_{\Phi_a(x)} \Omega \rightarrow \Lambda^2 T_{\Phi_a(x)} \Omega$$

be the curvature operator of g . For any simple 2-form $u \wedge v \neq 0$, one has

$$K_g(u \wedge v) = \frac{\langle \mathcal{R}(u \wedge v), u \wedge v \rangle}{\|u \wedge v\|^2} \quad (64)$$

In $m = 3$, choose the orthonormal basis of $\Lambda^2 T_{\Phi_a(x)} \Omega$:

$$\sigma_1 := e_2 \wedge e_3, \quad \sigma_2 := e_3 \wedge e_1, \quad \sigma_3 := e_1 \wedge e_2.$$

In this basis, \mathcal{R} is represented by a symmetric 3×3 matrix M . The diagonal entries are exactly the sectional curvatures:

$$M_{11} = K_g(e_2 \wedge e_3), \quad M_{22} = K_g(e_3 \wedge e_1), \quad M_{33} = K_g(e_1 \wedge e_2) \quad (65)$$

The off-diagonals come from polarization. For example, consider

$$\xi := \frac{1}{\sqrt{2}}(\sigma_2 - \sigma_3) = \frac{1}{\sqrt{2}}((e_3 \wedge e_1) - (e_1 \wedge e_2))$$

Then by Eq. (64),

$$K_g(\xi) = \frac{\langle \mathcal{R}\xi, \xi \rangle}{\|\xi\|^2} = \frac{1}{2}(M_{22} + M_{33} - 2M_{23}) \quad (66)$$

$$\implies M_{23} = \frac{1}{2}(M_{22} + M_{33} - K_g(\xi))$$

Similar linear combinations recover M_{12} and M_{13} . Thus, knowing all relevant sectional curvatures (including such mixed directions ξ) determines M .

Now replace each smooth curvature in Eq. (65)–Eq. (66) by the corresponding discrete estimates $\widehat{K}_{ij,a}(x;r)$ (and the obvious discrete analogues for $K_g(\xi)$ obtained by applying the same tube construction to the appropriate linear combination of planes). Call the result $\widehat{M}_a(x;r)$.

Theorem 7.4 (Reconstruction of the curvature operator in 3D). *Under (H1)–(H5), let $\widehat{M}_a(x;r)$ be obtained from $\widehat{K}_{ij,a}(x;r)$ as above. Then, for any $a \rightarrow 0$, $r \rightarrow 0$ with $a/r \rightarrow 0$, we have*

$$\lim_{\substack{a \rightarrow 0, r \rightarrow 0 \\ a/r \rightarrow 0}} \widehat{M}_a(x;r) = M(\Phi_a(x)) \quad \text{entrywise}$$

Proof. Entrywise convergence follows from Corollary 7.2 applied to each required sectional curvature direction.

For example, M_{11} is $K_g(e_2 \wedge e_3)$ by Eq. (65), and the discrete proxy is $\widehat{K}_{23,a}(x;r)$. Corollary 7.2 gives

$$|\widehat{K}_{23,a}(x;r) - K_g(e_2 \wedge e_3)(\Phi_a(x))| \leq C \left(\frac{a}{r} + r \right) \xrightarrow{a \rightarrow 0, r \rightarrow 0, a/r \rightarrow 0} 0$$

So $\widehat{M}_a(x;r)_{11} \rightarrow M_{11}(\Phi_a(x))$. Similarly for M_{22} and M_{33} .

For M_{23} , we use Eq. (66). Define a discrete estimator $\widehat{K}_{\xi,a}(x;r)$ by taking $\xi = (\sigma_2 - \sigma_3)/\sqrt{2}$, i.e. we center a tube around the 2D surface whose tangent 2-plane at $\Phi_a(x)$ is spanned by $(e_3 \wedge e_1) - (e_1 \wedge e_2)$ (normalized), and we run the same tube-restricted counting construction. Corollary 7.2 again implies

$$\widehat{K}_{\xi,a}(x;r) \rightarrow K_g(\xi)(\Phi_a(x))$$

Plugging the discrete quantities into

$$M_{23} = \frac{1}{2} (M_{22} + M_{33} - K_g(\xi))$$

(and the analogous formulas for M_{12}, M_{13}) yields $\widehat{M}_a(x;r)_{23} \rightarrow M_{23}(\Phi_a(x))$ and similarly for the other off-diagonals. Thus every entry of $\widehat{M}_a(x;r)$ converges to the corresponding entry of $M(\Phi_a(x))$. \square

Finally, Ric and R are obtained via standard contractions. In 3D, for example,

$$\text{Ric}(e_1, e_1) = K_g(e_1 \wedge e_2) + K_g(e_1 \wedge e_3). \quad (67)$$

$$R = 2(K_g(e_1 \wedge e_2) + K_g(e_1 \wedge e_3) + K_g(e_2 \wedge e_3)) \quad (68)$$

We therefore define the *counts-only* Ricci and scalar estimators

$$\widehat{\text{Ric}}_a(e_1, e_1; x; r) := \widehat{K}_{12,a}(x;r) + \widehat{K}_{13,a}(x;r),$$

$$\widehat{R}_a(x;r) := 2(\widehat{K}_{12,a}(x;r) + \widehat{K}_{13,a}(x;r) + \widehat{K}_{23,a}(x;r)) \quad (69)$$

and similarly for $\text{Ric}(e_2, e_2)$ and $\text{Ric}(e_3, e_3)$.

By Corollary 7.2 and Theorem 7.4,

$$\widehat{\text{Ric}}_a(e_i, e_i; x; r) \rightarrow \text{Ric}_g(e_i, e_i)(\Phi_a(x)) \quad \text{as } a \rightarrow 0, r \rightarrow 0, a/r \rightarrow 0$$

$$\widehat{R}_a(x;r) \rightarrow R_g(\Phi_a(x)) \quad \text{as } a \rightarrow 0, r \rightarrow 0, a/r \rightarrow 0$$

Key point. All the raw inputs in $\widehat{K}_{ij,a}$, $\widehat{\text{Ric}}_a$, and \widehat{R}_a come from counting cells inside carefully chosen regions, always using the same yardstick (one crossing = one unit). The smooth metric $g = e^{2u}g_0$ is only used to interpret what those counts converge to and to prove rates.

8. SCALAR CURVATURE FROM COUNTS ALONE

Fix $m \geq 2$. Let X_a be a locally finite cell complex with intrinsic (count) metric d_h , one face crossing = 1. For a base cell x and an intrinsic radius $r \in \mathbb{N}$, write

$$B_{d_h}(x, r) := \{c : d_h(x, c) \leq r\}, \quad |B_{d_h}(x, r)| := \#B_{d_h}(x, r) \quad (70)$$

Let $\beta_m > 0$ be the fixed m -dimensional calibration constant for the chosen baseline adjacency (so that in the undeformed reference lattice, a ball of intrinsic radius r contains $\beta_m r^m$ cells; see App. A). We define two operational quantities.

(i) Reconstructed radius. The *reconstructed m -volume radius* at scale r is

$$(r_c^{(m)}(x; r))^m := \frac{|B_{d_h}(x, r)|}{\beta_m} \quad (71)$$

This is the radius one would *infer* from the observed count $|B_{d_h}(x, r)|$ if space were undeformed and perfectly baseline.

(ii) Local density. The *local space density* at scale r is

$$\rho_a(x; r) := \frac{|B_{d_h}(x, r)|}{\beta_m r^m} = \frac{(r_c^{(m)}(x; r))^m}{r^m} d \quad (72)$$

Thus $\rho_a(x; r) = 1$ on an undeformed baseline lattice, $\rho_a(x; r) > 1$ for local compression (more cells than baseline in the same count radius), and $\rho_a(x; r) < 1$ for local dilation.

To convert this purely volumetric information into a curvature signal, we compare r (the measured count radius) and $r_c^{(m)}(x; r)$ (the reconstructed radius from the same data), rescaled to remove the trivial r -dependence. Define the *normalized small-ball estimator*

$$K_{h,R}^{(m)}(x; r) := 6(m+2) \frac{r^m - (r_c^{(m)}(x; r))^m}{r^{m+2}} \quad (73)$$

Using Eq. (72),

$$(r_c^{(m)}(x; r))^m = \rho_a(x; r) r^m$$

so

$$r^m - (r_c^{(m)}(x; r))^m = r^m(1 - \rho_a(x; r)) \quad (74)$$

and therefore Eq. (73) becomes

$$K_{h,R}^{(m)}(x; r) = 6(m+2) \frac{r^m(1 - \rho_a(x; r))}{r^{m+2}} = 6(m+2) \frac{1 - \rho_a(x; r)}{r^2} \quad (75)$$

Equation Eq. (75) is *purely counts*. For each x and scale r we: (i) take the intrinsic ball $B_{d_h}(x, r)$, (ii) count its cells, (iii) compute $\rho_a(x; r)$ from Eq. (72), (iv) insert $\rho_a(x; r)$ into Eq. (75). No coordinates, no angles, no derivatives, and no shape assumptions are needed to *measure* $K_{h,R}^{(m)}(x; r)$. It is all counts. The smooth metric $g = e^{2u}g_0$ only appears in the interpretation of the limit and in the proof of the error bound Eq. (76) below.

We now state the convergence result. Let $\Omega \subset \mathbb{R}^m$ be open, let $u \in C^2(\Omega)$, and let $g = e^{2u}g_0$ be the conformal metric on Ω . For each mesh scale $a > 0$, let X_a be a locally finite complex with realization map $\Phi_a : X_a \rightarrow \Omega$ and per-cell weight v_a satisfying (H1)–(H5) on a given compact $K \Subset \Omega$ (Sec. 3). Write R_g for the scalar curvature of (Ω, g) .

Theorem 8.1 (Counts-only scalar curvature). *Let $K \Subset \Omega$ and assume (H1)–(H5) hold on K , with $\beta_m = \omega_m$ (Euclidean unit-ball volume) in Eq. (71)–Eq. (72). Then there exist constants $C_1, C_2 > 0$, depending only on the shape/degree bounds in (H1)–(H2) and on $\|u\|_{C^2(K)}$, such that for every $x \in X_a$ with $\Phi_a(x) \in K$ and every admissible intrinsic radius r ,*

$$|K_{h,R}^{(m)}(x; r) - R_g(\Phi_a(x))| \leq C_1 \frac{a}{r} + C_2 r \quad (76)$$

In particular, if $a \rightarrow 0, r \rightarrow 0$, and $a/r \rightarrow 0$, then

$$K_{h,R}^{(m)}(x; r) \rightarrow R_g(\Phi_a(x)) \quad \text{uniformly for } \Phi_a(x) \in K. \quad (77)$$

Proof. We sketch the argument; all steps are local on K and constants are uniform on K .

(1) *Count ball vs. g -ball.* By (H4) there exist $c_1, c_2 > 0$ such that for any $x \in X_a$ with $\Phi_a(x) \in K$ and any admissible r ,

$$B_g(\Phi_a(x), ar - c_1a) \subseteq \Phi_a(B_{d_h}(x, r)) \subseteq B_g(\Phi_a(x), ar + c_2a) \quad (78)$$

Thus the intrinsic count ball of radius r sits between two g -metric balls of radii $\rho_{\pm} = ar \pm O(a)$.

(2) *Volume quadrature.* By (H5), $v_a(\{c\})$ is uniformly comparable to the g -volume of cell c , so summing v_a over $B_{d_h}(x, r)$ approximates $\text{Vol}_g(B_g(\Phi_a(x), \rho))$ up to $O(a\rho^{m-1})$ for $\rho \asymp ar$. Since $|B_{d_h}(x, r)|$ and $v_a(B_{d_h}(x, r))$ differ only by the uniform per-cell weight in (H5), this gives a first-order control of $|B_{d_h}(x, r)|$ by $\text{Vol}_g(B_g(\Phi_a(x), ar))$.

(3) *Small-ball expansion.* For a smooth g , the g -volume of a small geodesic ball satisfies

$$\text{Vol}_g(B_g(y, \rho)) = \omega_m \rho^m - \omega_m \frac{R_g(y)}{6(m+2)} \rho^{m+2} + O(\rho^{m+3}), \quad \rho \downarrow 0$$

uniformly for y in K . Taking $\rho = ar$ and using Eq. (78) and step (2), we obtain

$$(r_c^{(m)}(x; r))^m = r^m - \frac{R_g(\Phi_a(x))}{6(m+2)} r^{m+2} + E(x; a, r) \quad (79)$$

with

$$|E(x; a, r)| \leq C(a r^{m-1} + r^{m+3})$$

where C depends only on K , (H1)–(H2), and $\|u\|_{C^2(K)}$.

(4) *Insert into the estimator.* Subtract Eq. (79) from r^m and multiply by $6(m+2)/r^{m+2}$:

$$K_{h,R}^{(m)}(x; r) = 6(m+2) \frac{r^m - (r_c^{(m)}(x; r))^m}{r^{m+2}} = R_g(\Phi_a(x)) + \tilde{E}(x; a, r)$$

where

$$|\tilde{E}(x; a, r)| \leq C_1 \frac{a}{r} + C_2 r$$

This is exactly Eq. (76), with C_1, C_2 depending only on the same data.

(5) *Limit.* If $a \rightarrow 0$, $r \rightarrow 0$, and $a/r \rightarrow 0$, then the right-hand side of Eq. (76) vanishes, which yields Eq. (77). \square

Equations Eq. (75), Eq. (76), and Eq. (77) give a complete intrinsic recipe:

- From *one* counting experiment at scale r (i.e. from $|B_{d_h}(x, r)|$ alone) we compute $\rho_a(x; r)$ and hence $K_{h,R}^{(m)}(x; r)$.
- $K_{h,R}^{(m)}(x; r)$ is dimensionally normalized and has the correct sign: it is positive when the local packing is tighter than the baseline calibration and negative when looser.
- Under refinement ($a \rightarrow 0$, $r \rightarrow 0$, $a/r \rightarrow 0$), this purely combinatorial quantity converges to the smooth scalar curvature R_g of the continuum relaxation $g = e^{2u}g_0$.

In summary,

$$K_{h,R}^{(m)}(x; r) = 6(m+2) \frac{1 - \rho_a(x; r)}{r^2} \longrightarrow R_g(\Phi_a(x))$$

and all inputs on the left are just counts of cells.

9. CONCLUSION

We presented an intrinsic, measurement-first geometry in which length is a count and curvature is the operational coefficient in the small-circle/small-ball mismatch observed with a one length unit that equals one cell crossing. Distances are defined purely by shortest face-crossing counts, and this count metric is geodesic on every locally finite complex. The resulting excess-radius diagnostics are assembled into unified small-ball/small-sphere estimators that (i) vanish on undeformed lattices, (ii) detect local contraction/dilation with the correct sign, and (iii) identify the smooth scalar curvature in the continuum limit.

Crucially, the scalar estimator $K_{h,R}^{(m)}(x; r)$, the directional sectional estimators $\hat{K}_{ij,a}(x; r)$, and their Ricci/trace combinations $\hat{\text{Ric}}_a$ and \hat{R}_a are obtained from *counts only*: one fixes a base cell, chooses an intrinsic radius, counts the cells in the corresponding intrinsic ball (or tube-restricted slice), and compares the measured radius to the reconstructed radius in the same gauge. No coordinates, no angles, no derivatives, and no shape assumptions are required to perform the measurement. The smooth metric $g = e^{2u}g_0$ enters only to interpret the limiting object and to prove error bounds: under mild regularity and mesh hypotheses we obtain uniform rates $O(a/r + r)$, and in the joint limit $a \rightarrow 0$, $r \rightarrow 0$, $a/r \rightarrow 0$ the discrete estimators converge to the Riemannian scalar curvature R_g , the sectional curvatures $K_g(e_i \wedge e_j)$, and hence to Ric_g itself.

The framework is therefore micro-agnostic and angle-free, yet admits a precise continuum interface. It provides a direct operational bridge from raw counts on a deforming cellular medium to standard curvature data of a smooth conformal relaxation $g = e^{2u}g_0$, with quantified stability (via small-ball rates) and convergence in the measured Gromov–Hausdorff sense.

A. BASELINE COUNTS AND CALIBRATIONS

This appendix fixes notation and removes the potential ambiguity between (i) the *adjacency-specific* lattice calibrations used for discrete diagnostics, and (ii) the *Euclidean* calibration used in the R -normalized estimator (cf. Sec. 6).

B. ADJACENCY-SPECIFIC BASELINE (DISCRETE DIAGNOSTICS)

For the ℓ^1 adjacency on \mathbb{Z}^m , the intrinsic ball and sphere counts are

$$|B_m(r)| = \sum_{k=0}^m 2^k \binom{m}{k} \binom{r}{k}, \quad |S_m(r)| = |B_m(r)| - |B_m(r-1)| \quad (80)$$

with the convention $\binom{r}{0} = 1$ and $\binom{r}{k} = 0$ for $k > r$. In particular:

$$\begin{aligned} m = 2: & \quad |S_2(r)| = 4r, \quad |B_2(r)| = 2r^2 + 2r + 1 \\ m = 3: & \quad |B_3(r)| = \frac{4}{3}r^3 + 2r^2 + \frac{8}{3}r + 1 \end{aligned}$$

and $|S_3(r)| = |B_3(r)| - |B_3(r-1)| = 4r^2 + 2$. Thus the undeformed lattice calibrations we use for *discrete* radius reconstruction are

$$\alpha_1^{\square} = 4, \quad \beta_2^{\square} = 2, \quad \beta_3^{\square} = \frac{4}{3}, \quad \beta_4^{\square} = \frac{2}{3}$$

(and analogously for hexagonal/cubic/hypercubic variants), so that $r_c^{(1)} = C_h/\alpha_1$, $r_c^{(2)} = \sqrt{A_h/\beta_2}$, $r_c^{(3)} = \sqrt[3]{V_h/\beta_3}$, etc.

Lemma B.1 (Derivation of Eq. (80)). *For $m \geq 1$ and $r \in \mathbb{N}$, $|B_m(r)| = \sum_{k=0}^m 2^k \binom{m}{k} \binom{r}{k}$.*

Proof. An integer vector $x \in \mathbb{Z}^m$ satisfies $\|x\|_1 \leq r$ iff exactly k coordinates are nonzero ($0 \leq k \leq \min\{m, r\}$), we choose which k coordinates in $\binom{m}{k}$ ways, choose their signs in 2^k ways, and distribute a sum $\leq r$ among k positive integers: the number of compositions of an integer $\leq r$ into k parts (allowing 0) equals $\binom{r}{k}$. Summing over k yields the formula. $|S_m(r)|$ is the forward difference $|B_m(r)| - |B_m(r-1)|$. \square

C. EUCLIDEAN CALIBRATION (FOR THE R -NORMALIZED ESTIMATOR)

When we identify the small-ball mismatch with the smooth scalar curvature, we normalize against the Euclidean volume $\alpha_m = \omega_m$:

$$\text{Vol}_g(B_g(x, r)) = \alpha_m r^m - \alpha_m \frac{R_g(x)}{6(m+2)} r^{m+2} + O(r^{m+3})$$

and therefore set $\beta_m = \alpha_m = \omega_m$ in the definition of the R -normalized estimator $K_{h,R}^{(m)}(x; r) = 6(m+2)(r^m - (r_c^{(m)})^m)/r^{m+2}$, so that $K_{h,R}^{(m)}(x; r) \rightarrow R_g(x)$ as $r \downarrow 0$ (Theorem 6.1).

Summary. Use $(\alpha_1^\square, \beta_m^\square)$ when comparing against the undeformed adjacency, and use $\beta_m = \omega_m$ when targeting R_g .

D. EXAMPLES ON VORONOI COMPLEXES

Let $\Omega \subset \mathbb{R}^m$ be open, $u \in C^2(\Omega)$, and $g = e^{2u}g_0$. For $h > 0$ let $\mathcal{P}_h \subset \Omega$ be a finite set that is quasi-uniform in g : there exist constants $0 < \delta \leq \Delta < \infty$ (independent of h) such that

$$\delta h \leq \text{dist}_g(p, \mathcal{P}_h \setminus \{p\}) \leq \sup_{x \in \Omega} \text{dist}_g(x, \mathcal{P}_h) \leq \Delta h \quad \text{for all } p \in \mathcal{P}_h \quad (81)$$

Let $\{V_p\}_{p \in \mathcal{P}_h}$ be the Voronoi tessellation in the g -metric, and let X_h be the cell complex whose cells are $\{V_p\}$ with face adjacency. Define $\Phi_h(V_p) := p$ and the count metric d_h on X_h as in Sec. 2. Let μ_h assign to each cell its g -volume, i.e. $\mu_h(\{V_p\}) = \text{Vol}_g(V_p)$, and set $\nu_h := \mu_h$ (so ν_h is volumetric).

Proposition D.1 (Voronoi complexes satisfy (H1)–(H5)). *Assume Eq. (81) and that u is C^2 with bounded derivatives on a compact $K \Subset \Omega$. Then, for h small enough, the Voronoi complex X_h with realization Φ_h and measure ν_h satisfies (H1)–(H5) on K with $a := h$.*

Proof. Fix $K \Subset \Omega$. Bounds in Eq. (81) imply g -balls of radius $\asymp h$ contain and are contained in each Voronoi cell intersecting K ; since u is C^2 on K , g and g_0 are bi-Lipschitz equivalent on K with constants independent of h . We verify the hypotheses.

(H1) *Local finiteness / degree bound.* If cells have inner/outer g -radii bounded by $c_1 h$ and $c_2 h$ uniformly on K (a consequence of Eq. (81)), then only $O(1)$ cells can meet a given V_p ; in particular, the face-degree is uniformly bounded, so the adjacency graph is locally finite.

(H2) *Shape regularity / mesh size.* For p with $V_p \cap K \neq \emptyset$, quasi-uniformity yields

$$B_g(p, c_1 h) \subset V_p \subset B_g(p, c_2 h)$$

hence $\text{diam}_{g_0}(V_p) \in [\tilde{c}_1 h, \tilde{c}_2 h]$ on K by bi-Lipschitz equivalence of g and g_0 .

(H3) *Coarse realization.* Φ_h is the identity on sites; the g_0 -distance between adjacent cell centers is $\leq Ch$ by the outer radius bound, hence the coarse realization and Ch -density on K follow.

(H4) *Ball inclusions.* Let $x \in X_h$ with $\Phi_h(x) \in K$. Any g -path of length L from $\Phi_h(x)$ intersects at most CL/h distinct Voronoi cells, because each traversal across a cell consumes at least the g -inradius $\geq c_1 h$. Therefore $d_h(x, y) \leq C d_g(\Phi_h(x), \Phi_h(y))/h$. Conversely, a shortest d_h -path of r cells has g -length $\geq c' r h$ since each step crosses a face at g -distance $\geq c' h$. Thus

$$B_g(\Phi_h(x), c' r h) \subseteq \Phi_h(B_{d_h}(x, r)) \subseteq B_g(\Phi_h(x), C r h)$$

which is the desired inclusion with $a = h$.

(H5) *Weight comparability.* On K , u is bounded C^2 , hence $\text{Vol}_g(V_p) \asymp h^m e^{mu(p)}$ uniformly over cells meeting K . Thus there is $\Lambda \geq 1$ with

$$\Lambda^{-1} h^m e^{mu(\Phi_h(V_p))} \leq \nu_h(\{V_p\}) \leq \Lambda h^m e^{mu(\Phi_h(V_p))}$$

All constants depend only on K, δ, Δ , and bounds on u and its derivatives on K , not on h . \square

Corollary D.2 (Directional and scalar convergence on Voronoi). *Under the assumptions of Proposition D.1, let $\hat{K}_{ij,h}(x; r)$ be the directional estimator computed from counts in an $O(h)$ -thick Fermi tube around the geodesic slice Σ_{ij} (as in Lemma 7.1), and let \hat{R}_m be the R -normalized small-ball estimator Eq. (42). Then for all x with $\Phi_h(x) \in K$ and all admissible r ,*

$$\begin{aligned} |\hat{K}_{ij,h}(x; r) - K_g(e_i \wedge e_j)(x)| &\leq C \left(\frac{h}{r} + r \right) \\ |\hat{R}_m(x; r) - R_g(\Phi_h(x))| &\leq C \left(\frac{h}{r} + r \right) \end{aligned}$$

and choosing $r \asymp \sqrt{h}$ yields error $O(\sqrt{h})$. The constants depend only on K , the quasi-uniformity parameters, and C^2 bounds for u on K .

Proof. Proposition D.1 verifies (H1)–(H5) with $a = h$. The bounds then follow from Theorem 5.1 (scalar) and Lemma 7.1 with its corollary (directional), observing that the same $O(h/r + r)$ rate holds uniformly on K . The minimizer of $h/r + r$ is $r = \sqrt{h}$, giving $O(\sqrt{h})$. \square

E. WORKED TOY: CONFORMAL BUMP VIA DENSITY

For $m \in \{2, 3\}$, let $\rho(x) = \exp(\varepsilon \varphi(x))$ with φ smooth, compactly supported, and ε small. Set $u = \frac{1}{m} \log \rho = \frac{\varepsilon}{m} \varphi$. The scalar curvature signal from density alone (Sec. 8) is

$$R(x) = \rho(x)^{-2/m} \left[-\frac{2(m-1)}{m} \frac{\Delta \rho}{\rho} + \frac{(m-1)(m+2)}{m^2} \frac{|\nabla \rho|^2}{\rho^2} \right]$$

To first order in ε this reduces to $R(x) = -\frac{2(m-1)}{m^2} \varepsilon \Delta \varphi(x) + O(\varepsilon^2)$. Sampling a quasi-uniform \mathcal{P}_h with respect to $g = e^{2u}g_0$ and forming the Voronoi complex X_h , Corollary D.2 with $r \asymp \sqrt{h}$ yields

$$\hat{R}_m(x; r) = R(x) + O(\sqrt{h}) + O(\varepsilon^2)$$

uniformly on compact sets inside the support of φ . This provides a crisp, non-lattice sanity check for the sign and localization of the estimator.

F. PROOF OF THE MEASURED GH LIMIT (THEOREM 3.1)

We prove convergence on compacts and then exhaust Ω . Throughout, C denotes a constant depending only on the data in (H1)–(H5) on the compact set under consideration (and may change from line to line).

Proposition F.1 (Local mGH on compacts). *Fix $K \Subset \Omega$. Under (H1)–(H5) on K , there exist $a_0 > 0$ and $C_K > 0$ such that for all $a \in (0, a_0]$ there is a correspondence $\mathcal{R}_a \subset X_a \times \Omega$ with*

$$\text{dis}(\mathcal{R}_a) \leq C_K a \quad (82)$$

and

$$d_P\left((\Phi_a)_\# v_a^K, \text{vol}_g^K\right) \leq C_K a \quad (83)$$

where d_P is the Prokhorov distance on probability measures, and

$$v_a^K := \frac{v_a \Phi_a^{-1}(K)}{v_a(\Phi_a^{-1}(K))}, \quad \text{vol}_g^K := \frac{\text{vol}_g(K)}{\text{vol}_g(K)} \quad (84)$$

Hence $(X_a, d_a^*, v_a) \rightarrow (\Omega, d_g, \text{vol}_g)$ in the measured GH sense on K .

Proof. Metric distortion bound. Choose $K' \Subset K$ with $\text{dist}_g(K', \partial K) \geq ca$ for some fixed $c > 0$. Set

$$\mathcal{R}_a := \{(x, \Phi_a(x)) : \Phi_a(x) \in K'\} \subset X_a \times \Omega. \quad (85)$$

By (H4), for any $x \in X_a$ with $\Phi_a(x) \in K'$ and any integer $r \geq 0$,

$$B_g(\Phi_a(x), ar - c_1 a) \subseteq \Phi_a(B_{d_h}(x, r)) \subseteq B_g(\Phi_a(x), ar + c_2 a) \quad (86)$$

Let $x, y \in X_a$ with $\Phi_a(x), \Phi_a(y) \in K'$. Taking the minimal $r = d_h(x, y)$ in Eq. (86) and comparing the infimum s such that $\Phi_a(y) \in B_g(\Phi_a(x), as + c_2 a)$ yields

$$\left| d_g(\Phi_a(x), \Phi_a(y)) - a d_h(x, y) \right| \leq Ca \quad (87)$$

Since $d_a^* = a d_h$, Eq. (87) implies

$$\sup_{(x,p),(y,q) \in \mathcal{R}_a} |d_g(p, q) - d_a^*(x, y)| \leq Ca \quad (88)$$

i.e. $\text{dis}(\mathcal{R}_a) \leq Ca$, proving Eq. (82) (with C_K in place of C).

Pushforward measure bound. Let $\psi \in C_c^\infty(K')$ with $\|\psi\|_{C^1(K)} \leq 1$. Using (H2)–(H5) and a per-cell Taylor estimate,

$$\begin{aligned} \int \psi d((\Phi_a)_\# v_a) &= \sum_{\substack{c \in \mathcal{C}_a \\ \Phi_a(c) \in K'}} \psi(\Phi_a(c)) v_a(\{c\}) \\ &= \int_{K'} \psi d\text{vol}_g + O_K(a) \end{aligned} \quad (89)$$

(Here the $O_K(a)$ depends only on shape/degree bounds and $\|u\|_{C^2(K)}$.) After normalizing to probabilities as in Eq. (84), the same estimate gives

$$\left| \int \psi d((\Phi_a)_\# v_a^K) - \int \psi d\text{vol}_g^K \right| \leq C_K a \quad (90)$$

Since $C_c^\infty(K')$ is dense in the bounded-Lipschitz class on K' and both measures are tight on K , Eq. (90) implies

$$d_{\text{BL}}\left((\Phi_a)_\# v_a^K, \text{vol}_g^K\right) \leq C_K a \quad (91)$$

The Prokhorov distance metrizes weak convergence on a compact metric space and is controlled by d_{BL} ; hence

$$d_P\left((\Phi_a)_\# v_a^K, \text{vol}_g^K\right) \leq C_K a \quad (92)$$

which is Eq. (83).

Conclusion on K . Combining Eq. (82) and Eq. (83) with the standard characterization of measured GH convergence via correspondences with small distortion and small pushed-measure discrepancy yields the claim on K . \square

Proof of Theorem 3.1. Let $\{K_n\}_{n \geq 1}$ exhaust Ω by compacts with smooth boundary. By Proposition F.1, for each fixed n ,

$$d_{\text{mGH}}\left((X_a, d_a^*, v_a)|_{K_n}, (\Omega, d_g, \text{vol}_g)|_{K_n}\right) \leq C_{K_n} a \quad (93)$$

A diagonal argument in n gives measured GH convergence locally uniformly on compacts, hence $(X_a, d_a^*, v_a) \xrightarrow{\text{mGH}} (\Omega, d_g, \text{vol}_g)$. \square

Funding. None.

Disclosures. The authors declare no conflicts of interest.

Data Availability. No datasets were generated or analyzed in this study.

REFERENCES

1. S. Barak, "Universe geometry of a deformed 3d space lattice," HAL archive (2025). HAL Id: hal-04670068.
2. A. Einstein, "On the method of theoretical physics," *Philos. Sci.* **1**, 163–169 (1934). Herbert Spencer Lecture, Oxford, 1933.
3. W. Rindler, *Relativity: Special, General, and Cosmological* (Oxford University Press, 2004).
4. T. Regge, "General relativity without coordinates," *Il Nuovo Cimento* **19**, 558–571 (1961).
5. D. Burago, Y. Burago, and S. Ivanov, *A Course in Metric Geometry*, vol. 33 of *Graduate Studies in Mathematics* (American Mathematical Society, 2001).
6. F. Morgan, *Riemannian Geometry: A Beginner's Guide* (A K Peters, 1998), 2nd ed.
7. M. P. do Carmo, *Riemannian Geometry* (Birkhäuser, 1992).
8. A. I. Bobenko and Y. B. Suris, *Discrete Differential Geometry: Integrable Structure* (American Mathematical Society, 2008).
9. P. Petersen, *Riemannian Geometry*, vol. 171 of *Graduate Texts in Mathematics* (Springer, 2016), 3rd ed.
10. R. M. Wald, *General Relativity* (University of Chicago Press, 1984).
11. C. W. Misner, K. S. Thorne, and J. A. Wheeler, *Gravitation* (W. H. Freeman, 1973).